© 2020. Published by The Company of Biologists Ltd | Journal of Cell Science (2021) 134, jcs246603. doi:10.1242/jcs.246603

RESEARCH ARTICLE

SPECIAL ISSUE: CELL BIOLOGY OF HOST–PATHOGEN INTERACTIONS

Proteomic and mechanistic dissection of the poxvirus-customized ribosome

Stephen DiGiuseppe[1], Madeline G. Rollins[1], Helen Astar[1], Natalia Khalatyan[2], Jeffrey N. Savas[2] and Derek Walsh[1,*]

ABSTRACT

Ribosomes are often viewed as protein synthesis machines that lack intrinsic regulatory capacity. However, studies have established that ribosomes can functionally diversify through changes in the composition of, or post-translational modifications to ribosomal subunit proteins (RPs). We recently found that poxviruses phosphorylate unique sites in the RP, receptor for activated C kinase 1 (RACK1) to enhance viral protein synthesis. Here, we developed approaches for large-scale proteomic analysis of ribosomes isolated from cells infected with different viruses. Beyond RACK1, we identified additional phosphorylation events within RPS2 and RPS28 that arise during poxvirus infection, but not other viruses tested. The modified sites lie within unstructured loop domains that position around the mRNA entry and exit channel, respectively, and site-substitution mutants revealed that each modified residue contributed differently to poxvirus replication. Our findings reveal the broader extent to which poxviruses customize host ribosomes and provide new insights into how ribosomes can functionally diversify.

KEY WORDS: Ribosome, RPS, Post-translational modification, Phosphorylation, Poxvirus

INTRODUCTION

The initiation of protein synthesis involves scanning of the mRNA 5′ untranslated region (UTR) by a small 40S ribosomal subunit that, upon recognition of a start codon, is joined by a large 60S ribosomal subunit to assemble a translationally competent 80S ribosome (Hinnebusch, 2014; Meade et al., 2019). The mammalian 80S ribosome consists of 80 core ribosomal proteins (RPs) in complex with four ribosomal RNAs (rRNAs) (Genuth and Barna, 2018; de la Cruz et al., 2015). The functions of individual RPs range from structural integrity of the ribosome and ensuring translational fidelity, to facilitating the binding of translation initiation, elongation and release factors (Hinnebusch, 2014). These latter regulatory factors are often credited with much of the translational decision making in terms of the specific mRNAs that are to be translated and the efficiency with which this occurs. Meanwhile, as a large macromolecular complex that translates an extremely diverse range of mRNA types with exquisite speed and accuracy, the ribosome itself is often viewed as a passive player in this process, operating largely as a 'decoding machine' that is instructed by outside factors (Genuth and Barna, 2018).

However, increasing lines of evidence support the concept of compositional heterogeneity and functional diversification of ribosomes as a means to control translation rates of different mRNA types (Genuth and Barna, 2018). Heterogeneity can arise in a number of ways, including defects in ribosome biogenesis that alter ribosome numbers and composition, as well as regulated changes in subunit composition or post-translational modifications (PTMs) to RPs (Simsek and Barna, 2017; Ferretti and Karbstein, 2019). In mammalian development and body planning, differential tissue expression of the large RP RPL38 directs translation of homeobox (HOX) mRNAs that harbor structural elements within their 5′ UTR that are similar to viral internal ribosome entry sites (IRESs) (Kondrashov et al., 2011; Shi and Barna, 2015; Shi et al., 2017). Indeed, viruses, with their absolute dependence on gaining access to host ribosomes, are proving to be powerful tools in uncovering examples of ribosome specification. RNAi-based screens have shown that dicistroviruses and hepatitis viruses, whose mRNAs harbor IRESs, rely more than host mRNAs on specific ribosomal proteins for efficient translation (Cherry et al., 2005; Majzoub et al., 2014). These include the small RPs, RPS25 and receptor for activated C kinase 1 (RACK1). Subsequent studies have shown that several of these RPs interact directly with the viral IRES elements, and likely facilitate their non-canonical cap-independent mode of translation (Nishiyama et al., 2007; Landry et al., 2009; Fuchs et al., 2015; Hertz et al., 2013; Majzoub et al., 2014; van de Waterbeemd et al., 2018). Similar genetic screens have shown that RPS25 is required for repeat-associated non-AUG (RAN) translation in both neurons and yeast (Yamada et al., 2019), further supporting the idea that specific RPSs selectively regulate non-canonical modes of translation in a range of biological contexts.

While these examples reveal tissue-specific differences in ribosome composition and differential dependencies of mRNAs for specific RPs, there is also emerging evidence for structural and functional heterogeneity across ribosomes within individual cells. The potential for this to occur is perhaps unsurprising given that cells contain, on average, around 10 million ribosomes, but precisely because of this complexity this concept has remained challenging to study. However, recent mass spectrometry studies suggest that some RPs are present on ribosomes at sub-stoichiometric levels and are associated with the translation of specific mRNAs in mammalian cells (Xue et al., 2015; Shi et al., 2017; van de Waterbeemd et al., 2018). In addition, mutations to specific ribosomal proteins are associated with disease conditions, or 'ribosomopathies'. Among these, studies have shown that ribosomes lacking RPS26 enhance translation of a subset of stress-related mRNAs (Ferretti et al., 2017). Interestingly, unlike in mammals, many RP genes are duplicated in yeast and stress can

[1]Department of Microbiology-Immunology, Feinberg School of Medicine, Northwestern University, Chicago, IL 60611, USA. [2]Department of Neurology, Feinberg School of Medicine, Northwestern University, Chicago, IL 60611, USA.

*Author for correspondence (derek.walsh@northwestern.edu)

D.W., 0000-0002-8756-4655

Handling Editor: Michael Way
Received 20 March 2020; Accepted 14 May 2020

Journal of Cell Science (2021) 134, jcs246603. doi:10.1242/jcs.246603

alter the expression and ribosome occupancy of RP paralogs, resulting in ribosome heterogeneity that affects translation (Komili et al., 2007; Ghulam et al., 2019). Beyond changes in RP levels in yeast, stress conditions are also unearthing evidence for the functional importance of PTMs in both yeast and mammals. Ubiquitylation of RPS3, RPS10 and RPS20 have been shown to function in the stalling of ribosomes that occurs on aberrantly polyadenylated [poly(A)] mRNAs during ribosome quality control (RQC), which subsequently triggers clearance of the defective mRNA and peptide (Juszkiewicz and Hegde, 2017; Sundaramoorthy et al., 2017; Simms et al., 2017; Garzia et al., 2017; Juszkiewicz et al., 2018). In addition, clearance of stalled mRNAs at the endoplasmic reticulum has been associated with RP ufmylation, a ubiquitin-like PTM (Xu and Barna, 2020; Simsek et al., 2017). Moreover, ufmylation has been found to facilitate the recruitment of ribosome-associated proteins (RAPs) that enable environmental signals to communicate with the ribosome (Simsek et al., 2017). However, despite the detection of several other PTMs on RPs, whether many of these exert functional effects remains unclear.

We recently uncovered an unusual form of ribosome customization that occurs during infection with the poxvirus, Vaccinia Virus (VacV), which involves unique phosphorylation events in the RP RACK1 that are driven by the virus-encoded B1 kinase (Jha et al., 2017). The phosphorylated residues lie within an unstructured loop domain in RACK1 that extends into the mRNA exit channel and enhances translation of viral mRNAs, which harbor unusual poly(A)-leaders in their 5′UTRs (Jha et al., 2017; Rollins et al., 2019). Such leaders are not normally found in mammalian mRNAs, but function as cap-independent translational enhancers during poxvirus infection in part through RACK1 phosphorylation (Dhungel et al., 2017; Rollins et al., 2019; Jha et al., 2017). Intriguingly, the introduction of phosphate by poxviruses into the human RACK1 loop serves to mimic negatively charged amino acids that are naturally present in the RACK1 loop domains of dicot plant species (Rollins et al., 2019), which use adenosine-rich leaders to enhance translation of immune response mRNAs (Xu et al., 2017). Poxviruses also appear to passively exploit RPS20 ubiquitylation by the E3 ligase ZNF598, which is normally associated with poly(A)-based activation of RQC but enhances viral protein synthesis during infection (DiGiuseppe et al., 2018). This suggests that translation of poxvirus mRNAs might be accommodated by broader exploitation of ribosomal modifications. Indeed, several studies offer hints that other ribosomal proteins may also be modified during poxvirus infection, but the nature of these modifications and their potential functional significance remain unknown (Banham et al., 1993; Kaerlein and Horak, 1978; Buendia et al., 1987). Here, we developed approaches to isolate and analyze the composition of ribosomes from cells infected with a number of DNA and RNA viruses. In doing so, we uncover phosphorylation events on RPS2 and RPS28 that occur specifically during infection by poxviruses and which exert differential effects on virus replication. These findings expand our understanding of the extent to which poxviruses customize ribosomes and provide new insights into the functionality of specific RPS domains and modifications in regulating translation.

RESULTS

There were three important considerations in how we developed our approach to isolate and analyze ribosomes from infected cells: (1) the choice of RP to tag, (2) the choice of tag to isolate ribosomes, and (3) the cell type to use. In terms of RP and tag choice, while several different RPs have been used to isolate ribosomes in previous studies (Shi et al., 2017; Sanz et al., 2009; Simsek et al., 2017), we used RACK1–eGFP (Fig. 1A) for several reasons. RACK1 is a tightly bound core subunit of the 40S ribosome that is present at stoichiometric levels and therefore present on most, if not all, ribosomes in the cell. In addition, RACK1 is rapidly degraded when it is not present on the ribosome in several cell types (Jha et al., 2017; Majzoub et al., 2014; Coyle et al., 2009; Schmitt et al., 2017; Johnson et al., 2019; Sengupta et al., 2004). As such, RACK1 should enable high affinity isolation of both scanning 40S and assembled 80S subunits. Although eGFP is a large tag, when combined with GFP-TRAP resins it offers clean, IgG-free isolation of complexes for subsequent mass spectrometry analysis. The location of RACK1 as a largely solvent-facing RP on the outer edge of the 40S subunit makes it readily amenable to C-terminal tagging with eGFP without affecting its functionality (Cox et al., 2002; Jha et al., 2017; Rollins et al., 2019; Sengupta et al., 2004) (Fig. 1A).

In terms of our choice of cell type, while RPs are often reported to have extra-ribosomal functions in several widely used transformed cell lines, we and many others have found that primary cells and certain cell lines restrict RPs to the ribosome through degradation of free (extra-ribosomal) subunits (Sung et al., 2016; Gallo et al., 2018; Romano et al., 2019; Jha et al., 2017; Ceci et al., 2003; Gerbasi et al., 2004; Johnson et al., 2019; Sengupta et al., 2004). For that reason, RACK1 cannot be overexpressed in primary normal human dermal fibroblasts (NHDFs), for example, as exogenously expressed forms must compete with endogenous RACK1 for stabilization through ribosome binding (Jha et al., 2017; Rollins et al., 2019). As such, exogenous RACK1 expression results in a concomitant downregulation of endogenous RACK1, maintaining a natural homeostatic level of RACK1 on the ribosome. However, isolation of sufficient material for extensive mass spectrometry is challenging using primary cells. Our approach therefore required a cell line that would provide sufficient material but which retained this homeostatic balance. HAP1 cells are a fibroblast-like near-haploid cell line that we previously used to generate a RACK1 knockout line (Jha et al., 2017), and which do not contain appreciable amounts of extra-ribosomal RACK1 or other RPs (LaFontaine et al., 2020). Studies of these cells by other groups have shown that exogenous re-expression of RACK1 rescues phenotypes studied and, importantly, RACK1 is tightly bound to the ribosome in these cells (Johnson et al., 2019; LaFontaine et al., 2020). In line with this, we found that when RACK1–eGFP was transduced into parental HAP1 cells only low levels of expression could be achieved relative to the endogenous form, and only equivalently small reductions in endogenous RACK1 were observed in RACK1–eGFP-expressing lines (Fig. 1B). However, in RACK1 knockout HAP1 cells, expression of RACK1–eGFP resulted in the restoration of RACK1 levels to those observed in the parental line. As such, we used RACK1-knockout HAP1 cells that had been rescued with RACK1–eGFP to ensure that our isolation approach sampled all ribosomes within the cell, and not a small subpopulation of tagged ribosomes, as would otherwise be isolated from parental lines.

Using these cells, we isolated ribosomes on GFP-TRAP resin from uninfected cells or cells infected with VacV. Silver staining showed the specificity of this approach, with little to no protein being detected in RACK1 knockouts that were not rescued with RACK1–eGFP (Fig. 1C). The pattern of stained proteins in complexes isolated from uninfected or infected cells did not exhibit any striking differences. To test this further, samples were processed and analyzed by liquid chromatography tandem mass

Journal of Cell Science (2021) 134, jcs246603. doi:10.1242/jcs.246603

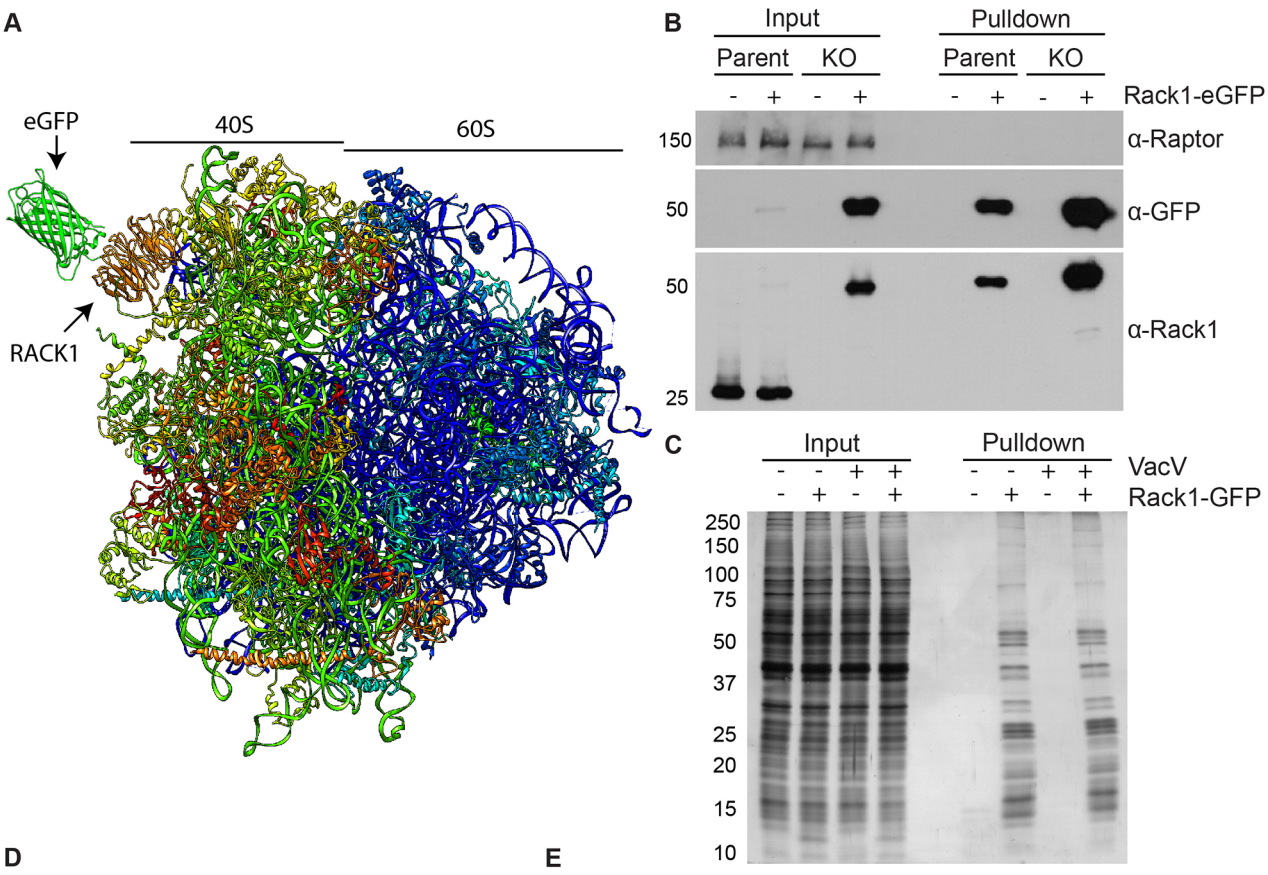

D

40S Small Ribosomal Subunit Proteins			
RACK1	RPS6	RPS15	RPS23
RPSA	RPS7	RPS15A	RPS24
RPS2	RPS8	RPS16	RPS25
RPS3	RPS9	RPS17	RPS26
RPS3A	RPS10	RPS17L	RPS27
RPS4X	RPS11	RPS18	RPS27L
RPS4Y1	RPS12	RPS19	RPS28
RPS4Y2	RPS13	RPS20	RPS29
RPS5	RPS14	RPS21	RPS30

60S Large Ribosomal Subunit Proteins			
RPLP0	RPL9	RPL19	RPL30
RPLP0P6	RPL10	RPL21	RPL31
RPLP1	RPL10A	RPL22	RPL32
RPLP2	RPL10L	RPL22L	RPL34
RPL3	RPL11	RPL23	RPL35
RPL3L	RPL12	RPL23A	RPL35A
RPL4	RPL13	RPL24	RPL36
RPL5	RPL13A	RPL26	RPL36A
RPL6	RPL14	RPL26L	RPL36A
RPL7	RPL15	RPL27	RPL37
RPL7A	RPL17	RPL27A	RPL37A
RPL7L	RPL18	RPL28	RPL38
RPL8	RPL18A	RPL29	

E

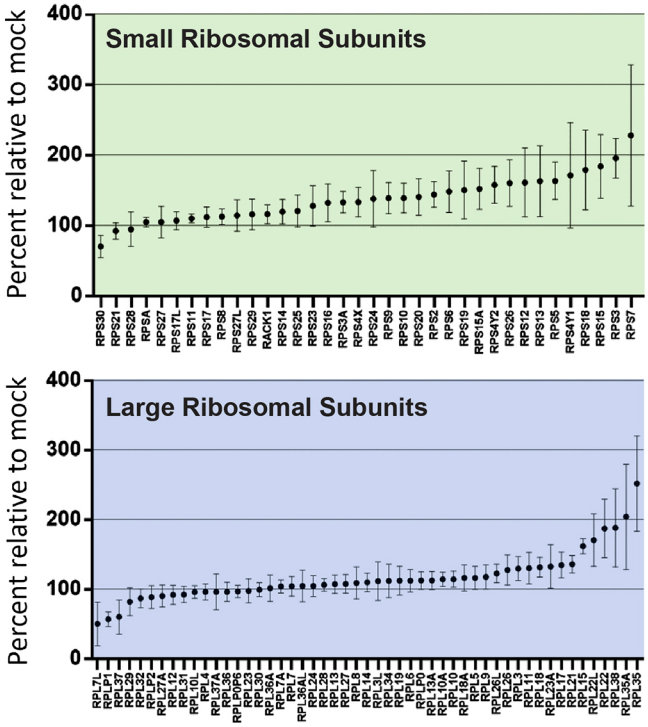

Fig. 1. Proteomic analysis of host ribosomes during poxvirus infection. (A) Structural model of the 80S ribosome, with 40S and 60S subunits indicated, showing RACK1–eGFP used for GFP–TRAP isolation. (B) Western blot analysis of RACK1 expression and isolation using GFP-TRAP in parental or RACK1-knockout (KO) HAP1 cells expressing empty vector (–) or RACK1–eGFP (+). Raptor serves as a loading and ribosome isolation specificity control. (C) Silver stain of cell lysates and GFP-TRAP-isolated ribosomes from uninfected or VacV infected (MOI=5) HAP1 knockout cells expressing empty vector (–) or RACK1–eGFP at 20 hpi. (D) RPSs (green) and RPLs (blue) identified by mass spectrometry following GFP-TRAP isolation of ribosomes from HAP1 cells expressing RACK1–eGFP that were either uninfected or infected with VacV (MOI=5). (E) Analysis of the spectral count ratios for indicated proteins comparing mock-infected and VacV-infected samples presented as mean±s.e.m. (*n*=5).

Journal of Cell Science (2021) 134, jcs246603. doi:10.1242/jcs.246603

spectrometry (LC-MS/MS). This analysis identified all of the expected RPSs and RPLs that make up the 80S ribosome (Fig. 1D). Further analysis of spectral counts to determine the ratios of the various RPs between mock and infected samples revealed no striking differences (Fig. 1E). This suggested that the subunit composition of the ribosome is mostly unchanged during poxvirus infection.

We next tested whether our LC-MS/MS analysis detected any phosphorylation events that were specific to infection by poxviruses, which are large cytoplasmically replicating DNA viruses. As controls for specificity to poxviruses, we extended our analysis to include cells infected by another large DNA virus, herpes simplex virus type 1 (HSV-1) and an RNA virus, Vesicular Stomatitis virus (VSV). Silver staining and LC-MS/MS analysis, albeit using peptide counts as a measure over more quantitative mass spectrometry approaches, suggested that there were no gross differences in subunit composition, and in particular no obvious loss or gain of RPs between uninfected cells or cells infected with any of the viruses tested (Fig. 2A). Analysis of phosphorylated peptides identified a modification to RPS3A across all infected samples, which might represent a stress response, as well as several shared modifications between two of the three viruses tested (Fig. 2B). However, of particular interest to us, several RPSs, RPLs and RAPs were found to be uniquely phosphorylated in VacV-infected cells. These included several ZNF family members, which was interesting given our recent discovery that ZNF598 and RPS20 ubiquitylation enhance poxvirus replication (DiGiuseppe et al., 2018). Of most interest to us at this time was the detection of RACK1 phosphorylation, in line with our prior findings (Jha et al., 2017), as well as phosphorylation of RPS2 and RPS28. These two latter proteins were of interest due to their position on the ribosome; RPS28 lies at the mRNA exit channel near RACK1, while RPS2 lies at the mRNA entry channel (Sengupta et al., 2004). RNAi-mediated depletion of either RPS2 or RPS28 was found to suppress the spread of VacV in parental HAP1 cells as determined by reduced accumulation of poxvirus proteins D8 and A14, without inducing markers of cellular stress, such as eIF2α phosphorylation or elevated expression of protein kinase R (PKR) or interferon stimulated gene 56 (ISG56; also known as IFIT1) (Fig. 2C,D). While this observation suggested that these two RPSs were important for poxvirus infection, we next validated and tested the functionality of the specific modifications to each protein.

Phosphorylation of two residues within RPS2 regulates poxvirus protein synthesis

Phosphorylation can cause shifts in the migration of some proteins when resolved by SDS-PAGE. While no such shifts could be detected for RPS28, western blot (WB) analysis of uninfected or infected parental HAP1 cells detected a slower migrating band on RPS2 blots in VacV-infected samples that was not evident in either uninfected cells or cells infected with HSV-1 or VSV (Fig. 3A). Probing for viral proteins demonstrated that these cells were indeed infected by each virus, in line with widespread cytopathic effect that we routinely observed in infected cells. However, the relatively high abundance of RPSs in HAP1 cells made it difficult to detect band-shifted species. As such, we tested whether RPS band-shifts might be more readily detectable in primary NHDFs, which express physiologically normal levels of proteins. In doing so, we found that although RPS28 again did not exhibit a notable band-shift, mobility changes were readily detected for RACK1, as we have reported previously (Jha et al., 2017), and for RPS2 (Fig. 3B). These mobility shifts were observed in VacV-infected cells, but not in mock, HSV-1 or VSV-infected cells. Phosphatase treatment of cell lysates resulted in a dose-dependent loss of the shifted RPS2 species (Fig. 3C), demonstrating that the mobility shift was indeed due to phosphorylation. Interestingly, RPS2 was one of two RPs that were previously identified 30 years ago as incorporating radiolabeled phosphate in the presence of the viral B1 kinase *in vitro*, but the sites that were modified and their potential functional importance remain unknown (Banham et al., 1993; Buendia et al., 1987; Kaerlein and Horak, 1978). To test whether the mobility shifts that we observed by WB were B1 dependent, we infected NHDFs with wild-type (WT) VacV or temperature sensitive mutants of the two VacV kinases B1 and F10 (Jha et al., 2017; Boyle and Traktman, 2004; Punjabi and Traktman, 2005; Rempel and Traktman, 1992; Wiebe and Traktman, 2007). Notably, although these mutants were originally selected for temperature-sensitive replication, the mutations in the B1 and F10 genes actually result in unstable, poorly expressed proteins at both permissive (32°C) and non-permissive (39.5°C) temperatures. In line with this, WB analysis showed that RPS2 mobility shifts could be detected in cells infected with WT or either of the F10 mutant viruses, but not in extracts from cells infected with either of the B1 mutants tested (Fig. 3D,E). It is important to note that enzymes often do not operate at optimal efficiency at temperatures outside of 37°C, which likely explains why less of the modified form of RPS2 was detected in both WT and F10 virus-infected samples. However, these observations are in agreement with prior *in vitro* studies showing that B1 modifies RPS2 at unique sites (Banham et al., 1993).

LC-MS/MS spectra identified a number of potentially unique RPS2 phosphorylation sites in VacV-infected cells (Fig. 3F,G; Fig. S1). However, as the spectral data suggested two modifications were likely but identified three potential sites (T276, T278 and S281), we could not determine with absolute certainty which of these residues were being phosphorylated. To map which of these threonine or serine residues were being phosphorylated, we turned to site-directed mutagenesis using an N-terminally HA-tagged form of RPS2 expressed in NHDFs. WB analysis revealed that expression of HA–RPS2, but not HA–RPS28, resulted in a concomitant downregulation of endogenous RPS2 (Fig. 3H). As such, homeostatic mechanisms that degrade extra-ribosomal RPs, such as RACK1 (Jha et al., 2017; Warner and McIntosh, 2009), seem likely to also regulate RPS2 at least in primary NHDFs, and effectively enabled exogenous expression of RPS2 to function as a form of protein knock-in or replacement strategy.

Using site-directed mutagenesis, we converted each of the potential phosphorylated serine or threonine residues identified by our mass spectrometry analysis into non-phosphorylatable alanine residues. We then generated pools of NHDFs stably expressing WT or alanine-substituted HA–RPS2 and mock infected or infected them with VacV at a high multiplicity of infection (MOI). In WT HA–RPS2-expressing cells, a low level of endogenous RPS2 could still be detected, and mobility shifts were observed for both endogenous and HA-tagged forms of RPS2 upon infection (Fig. 3I). While mutant forms of exogenous RPS2 were expressed at slightly higher levels, such that endogenous protein was difficult to detect, the T276A mutant exhibited a mobility shift that was similar to that seen for WT HA–RPS2. By contrast, no mobility shift could be detected in cells expressing HA–RPS2 with either T278A or S281A mutations (Fig. 3I). This suggested that both of these sites were modified during poxvirus infection and contributed to the mobility shift observed by SDS-PAGE. WB analysis of viral proteins confirmed that all cells were equally infected with VacV, but also showed no notable defect in the accumulation of viral proteins

Journal of Cell Science (2021) 134, jcs246603. doi:10.1242/jcs.246603

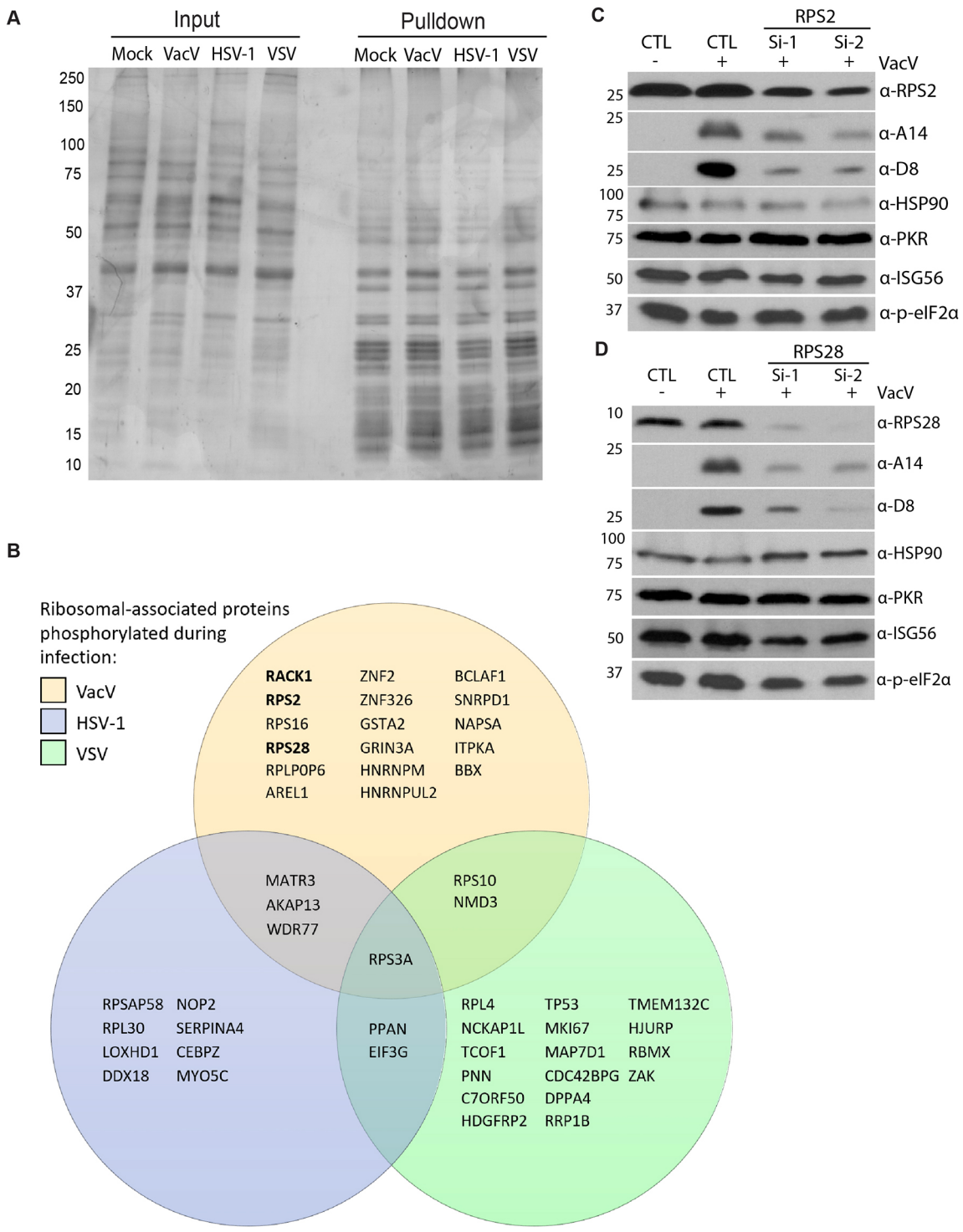

Fig. 2. Detection of phosphorylated ribosome-associated proteins during viral infections. (A) Silver stain of GFP-TRAP complexes from uninfected or VacV-, HSV-1- or VSV-infected (MOI=5) HAP1 cells expressing RACK1–eGFP at 20 hpi (for VacV and HSV-1) or 6 hpi (for VSV). (B) Venn diagram of ribosome-associated proteins identified by mass spectrometry of GFP-TRAP complexes as being uniquely phosphorylated in one or more infected sample, but not in uninfected samples. (C,D) Western blot analysis of samples from HAP1 cells depleted of RPS2 or RPS28 using two independent siRNAs (Si-1, Si-2) following infection with VacV (MOI=0.5) for 20 hpi (n=3). D8 and A14 are poxvirus proteins used to measure infection levels. Heat-shock protein HSP90 serves as a loading control.

tested. It is important to consider that PTMs to individual ribosomal proteins are likely to have subtle regulatory effects that contribute to overall viral protein production in conjunction with other modifications to the ribosome as well as to regulatory initiation factors, such as the cap-binding protein eIF4E (Walsh et al., 2008; Walsh and Mohr, 2004). Indeed, when studying eIF4E phosphorylation in isolation, its subtle stimulatory effects are masked due to the high levels of protein synthesis that occur at a high MOI. However, its importance becomes apparent in low MOI spreading assays, where small defects in protein synthesis in the

Journal of Cell Science (2021) 134, jcs246603. doi:10.1242/jcs.246603

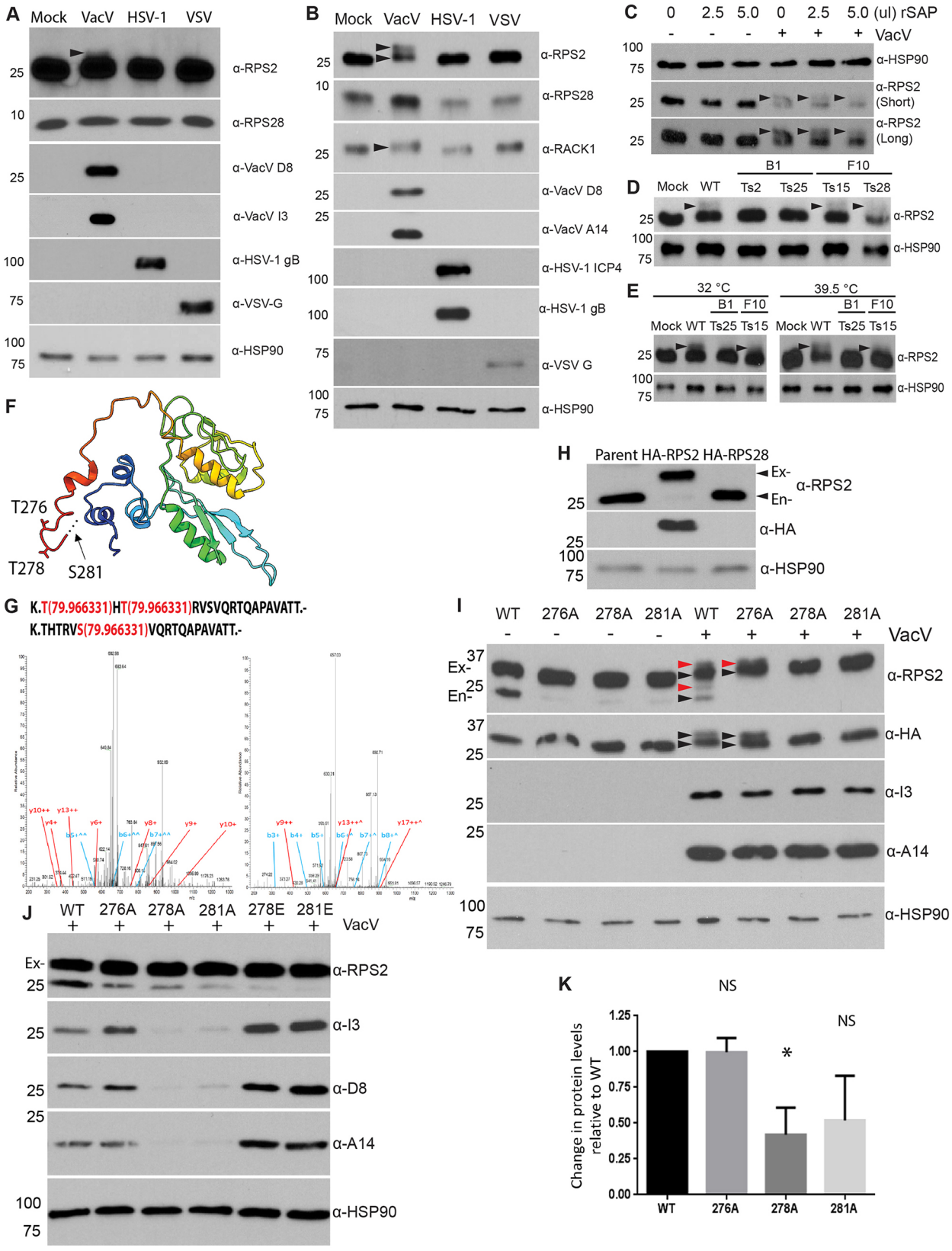

Fig. 3. See next page for legend.

absence of eIF4E phosphorylation have cumulative effects on virus replication and spread (Walsh et al., 2008). As such, we tested whether RPS2 mutants impacted the accumulation of viral proteins when cultures were infected at a low MOI for 3 days. In doing so, we found that levels of viral proteins were relatively unaffected in cells expressing HA–RPS2 harboring the T276A mutation compared

Journal of Cell Science (2021) 134, jcs246603. doi:10.1242/jcs.246603

Fig. 3. Threonine 278 and serine 281 of RPS2 are phosphorylated during VacV infection. (A) Western blot analysis of HAP1 cells infected with VacV, HSV-1 or VSV (MOI=5) at 20 hpi (for VacV and HSV-1) or 6 hpi (for VSV). Arrowheads point to bandshifted species. (B) Western blot analysis of NHDFs infected with VacV, HSV-1, or VSV (MOI=5) at 20 hpi (for VacV and HSV-1) or 6 hpi (for VSV). Arrowheads point to bandshifted species. (C) Western blot analysis of NHDF lysates that were either mock infected (–) or infected with VacV (+), then treated with recombinant shrimp alkaline phosphatase (rSAP) as indicated. Arrows point to the loss of band-shifted RPS2 in SAP-treated samples. (D,E) NHDFs infected with temperature sensitive (Ts) viral mutants of B1 or F10 kinase for 20 h at permissive (32°C) or non-permissive (39.5°C) temperatures. (F) Structural model of RPS2 with labeled amino acid residues identified as being phosphorylated during VacV infection. (G) MS/MS spectra of RPS2 peptides from GFP-TRAP ribosomes isolated from VacV-infected HAP1 cells. The peptide amino acid sequence, phosphorylated residue, b-series ions (blue), y-series ions (red), charge state (+), and ions that support phosphorylation (^) are all indicated. (H) Western blot analysis of NHDFs expressing HA–RPS2 or HA–RPS28 protein. Ex, exogenous RPS2; En, endogenous RPS2. (I) Western blot analysis of NHDFs expressing HA–RPS2 or site-specific alanine substitution mutants (T276A; T278A; S281A) infected with VacV (MOI=5) for 20 h. Exogenous and endogenous forms of RPS2 are indicated. Arrowheads point to unmodified (black) and modified (red) forms of each. (J) Western blot analysis of NHDFs expressing HA–RPS2 or site-specific alanine (T278A; S281A) or glutamic acid (T278E; S281E) substitution mutants infected with VacV (MOI=0.003) for 72 h. (K) Quantification of relative change in viral protein levels presented as mean± s.e.m. (*n*=4) of NHDFs expressing HA–RPS2 or site-specific alanine mutants (T276A; T278A; S281A) infected with VacV (MOI=0.003) for 72 h. **P*<0.05; NS, not statistically significant (unpaired Student's *t*-test).

with WT HA–RPS2 controls, while clear reductions in viral protein levels of ∼50% were observed in both the T278A- and S281A-expressing NHDF pools (Fig. 3J,K). Variability in effect size resulted in a lack of statistical significance for the S281A mutant, but the trend of reduced viral protein accumulation with this mutant was none-the-less consistent. It is important to consider the limitations of what statistics tell us in complex biological systems where processes naturally vary in effect size, as our data clearly shows the biological significance of phosphorylating S281 with regard to virus spread. However, this data, along with data presented below, hints at the idea that T278 might be the more functionally dominant modification site in RPS2. Regardless, both alanine-substituted mutants that prevented the RPS2 mobility shift observed by WB also negatively impacted VacV protein production during virus spread, revealing that the actively modified and functionally important sites in RPS2 were T278 and S281.

Next, we tested whether the defects caused by these alanine substitution mutations could be rescued by inserting negatively charged amino acids, mimicking the negatively charged phosphate introduced by VacV. To do this, we generated pools of NHDFs that expressed HA–RPS2 wherein the functionally important threonine and serine residues were replaced with glutamic acid; T278E and S281E. In the same low MOI spreading assays, while the T278A and S281A mutants reduced viral protein accumulation, VacV spread was not only restored but was in some instances modestly increased in NHDFs expressing the T278E or S281E phosphomimetics (Fig. 3J). Results using the T278E or S281E phosphomimetics varied between no significant enhancement or moderate increases in viral protein abundance compared to WT RPS2 (1/4 and 3/4 experiments, respectively), but importantly in no instance were reductions in viral proteins observed. As we discuss again later, detecting enhancer activity of phosphomimetic forms of RPS2 in this assay is complicated by the fact that the virus is naturally phosphorylating the WT form of HA–RPS2 in controls, meaning that both control and phosphomimetic conditions are comparable in the context of infection.

While these approaches identified the modified sites in RPS2 and their individual importance to efficient VacV replication, our mass spectrometry detected both modifications on the same peptide, demonstrating that T278 and S281 were simultaneously modified during infection. As such, we next tested the combined effect of both modifications on infection. To do this, we generated pools of NHDFs that expressed HA-tagged RPS2 with single glutamic acid substitutions at each site (T278E; S281E) or with both sites converted into either alanine (AA) or glutamic acid (EE) residues. Low MOI spreading assays and quantification of viral protein accumulation showed that preventing RPS2 phosphorylation at both sites, in cells expressing the T278A/S281A mutant, resulted in a 75% reduction in protein accumulation compared to that seen in cells expressing WT HA–RPS2, suggesting cumulative effects of preventing both sites from being modified (Fig. 4A,B). By contrast, viral protein accumulation was either unaffected or was modestly increased in NHDFs expressing the single-site or T278E/S281E phosphomimetics of RPS2. Furthermore, beyond viral protein accumulation, production of infectious virus was similarly decreased by ∼50% in cells expressing the HA–RPS2 T278A/S281A mutant (Fig. 4C). Similar to effects on viral protein accumulation, the T278E/S281E phosphomimetic supported normal levels of virus production. Overall, these data suggest that phosphorylating both T278 and S281 in RPS2 is important for maximal VacV protein production and virus spread.

As mentioned earlier, reliably detecting potential enhancer activity of the phosphomimetic forms of HA–RPS2 is complicated in the context of infection as the virus will naturally phosphorylate WT HA–RPS2 in controls, along with the other site that remains in single-site mutants. As such, we tested the effects of phosphomimetic forms of HA–RPS2 on translation outside the context of infection. To assess potential effects on overall translation, NHDF pools were pulsed with [^{35}S]methionine and [^{35}S]cysteine. SDS-PAGE fractionation and analysis of nascent proteins by autoradiography showed no notable difference in overall rates of translation or in the production of specific proteins in NHDFs expressing either single or double phosphomimetic forms of HA–RPS2 compared with WT HA-RPS2 (Fig. 4D). Quantification of ^{35}S incorporation by scintillation counting further showed no significant differences in overall rates of translation across these cells (Fig. 4E). Next, we tested whether negative charge in RPS2 affected protein production from mRNAs with a 5′ poly(A) leader, which is present on most poxvirus mRNAs. To do this, NHDFs expressing WT, single or double phosphomimetic forms of HA–RPS2 were electroporated with a luciferase reporter harboring a 5′ poly(A) leader (Jha et al., 2017; Rollins et al., 2019). Assays revealed that the insertion of single phosphomimetic residues at either T278 or S281 did not significantly enhance luciferase production compared with WT HA–RPS2 (Fig. 4F). However, NHDFs expressing HA–RPS2 harboring double T278E/S281E phosphomimetic mutations showed a statistically significant increase in luciferase activity of ∼30%. We did not measure RNA levels in these assays as increased translation rates can increase the stability of mRNAs, and therefore confounds any conclusions as to whether these effects are purely at the translational level. However, in this more controlled context these data suggest that phosphorylation of both T278 and S281, in tandem, is functionally important for maximal protein production from mRNAs that contain 5′ poly(A) leaders. This is in line with the effects of single and double alanine substitution mutants in the context of infection, and offers a functional explanation as to why the virus modifies both of these sites in RPS2.

Journal of Cell Science (2021) 134, jcs246603. doi:10.1242/jcs.246603

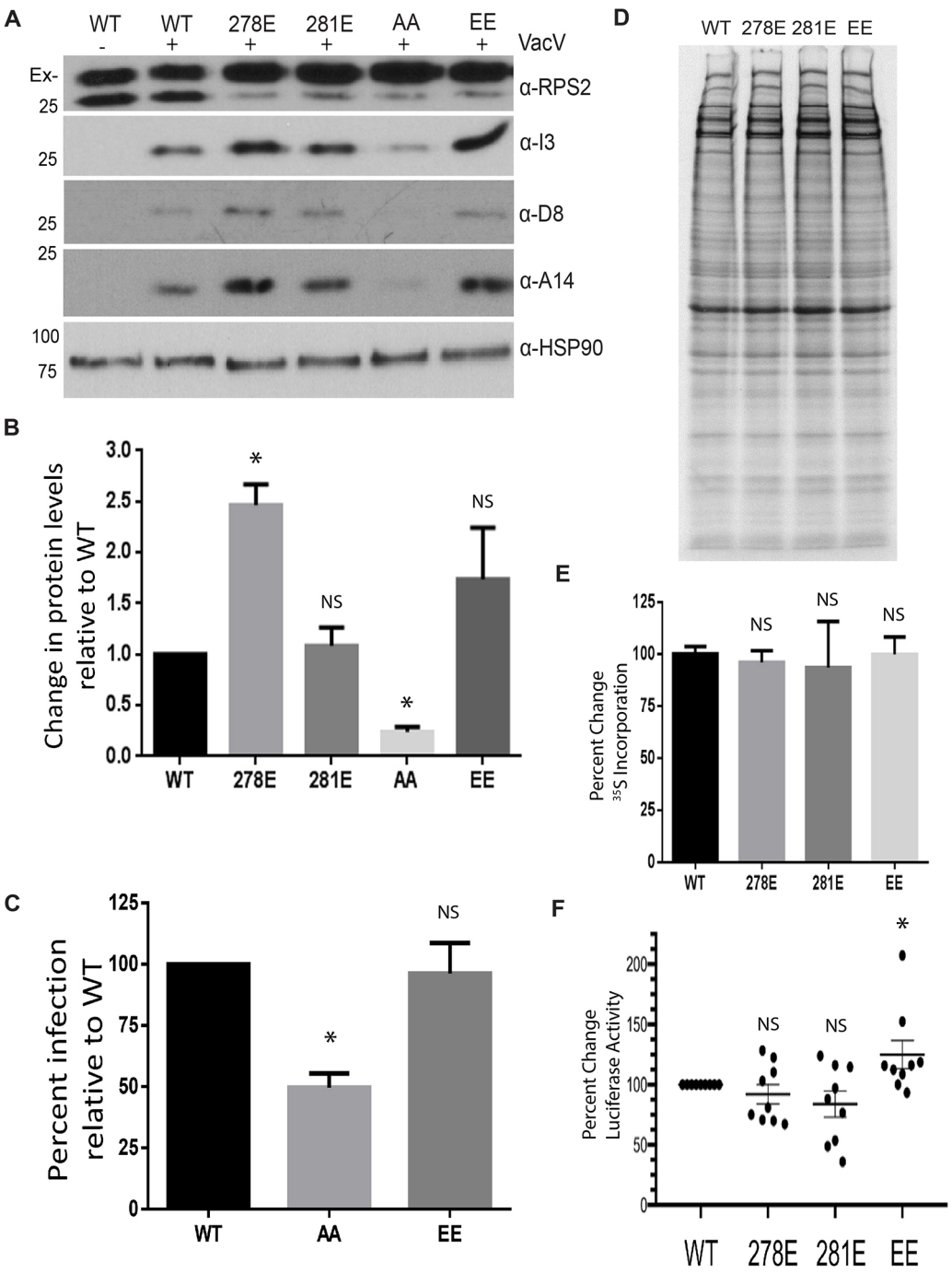

Fig. 4. Phosphorylation of both sites in RPS2 maximizes poxvirus protein synthesis and spread. (A) Western blot analysis of NHDFs expressing HA–RPS2 or site-specific glutamic acid (T278E; S281E), double alanine (AA), or double glutamic acid (EE) substitution mutants infected with VacV (+, MOI=0.003) for 72 h. (B) Quantification of relative change in viral protein levels presented as mean±s.e.m. (*n*=8) of NHDFs expressing HA–RPS2 or site-specific glutamic acid (T278E; S281E), double alanine (AA) or double glutamic acid (EE) substitution mutants infected with VacV (MOI=0.003) for 72 h. (C) Quantification of viral titers from NHDFs expressing HA–RPS2, or double alanine (AA) or glutamic acid (EE) substitution mutants of HA–RPS2 infected with VacV (MOI=0.003) for 72 h. Data is presented as mean±s.e.m. percentage infection relative to WT infection (*n*=4). (D) Autoradiography of [^{35}S]Met/Cys pulse-labeled NHDFs expressing HA–RPS2 or single or double glutamic acid (EE) substitution mutants. (E) Quantification of ^{35}S incorporation as determined by scintillation counting presented as mean±s.e.m. percentage (*n*=3) relative to WT. (F) Percentage change in luciferase activity from poly(A)-leader reporter in NHDFs expressing site-specific single glutamic acid (T278E; S281E) or double glutamic acid (EE) mutations presented as the mean±s.e.m. percentage relative to WT (*n*=9). **P*<0.05; NS, not statistically significant (unpaired Student's *t*-test).

RPS28 phosphorylation does not regulate VacV infection in NHDFs

We next tested whether the phosphorylation events in RPS28 that we detected were also functionally important. In this instance, spectral data suggested that RPS28 was uniquely phosphorylated at a single site in VacV-infected cells but, because of their proximity, we could not discern with certainty whether this occurred at T38 or S39 (Fig. 5A,B; Fig. S2). Unfortunately, unlike RPS2, RPS28 did

Journal of Cell Science (2021) 134, jcs246603. doi:10.1242/jcs.246603

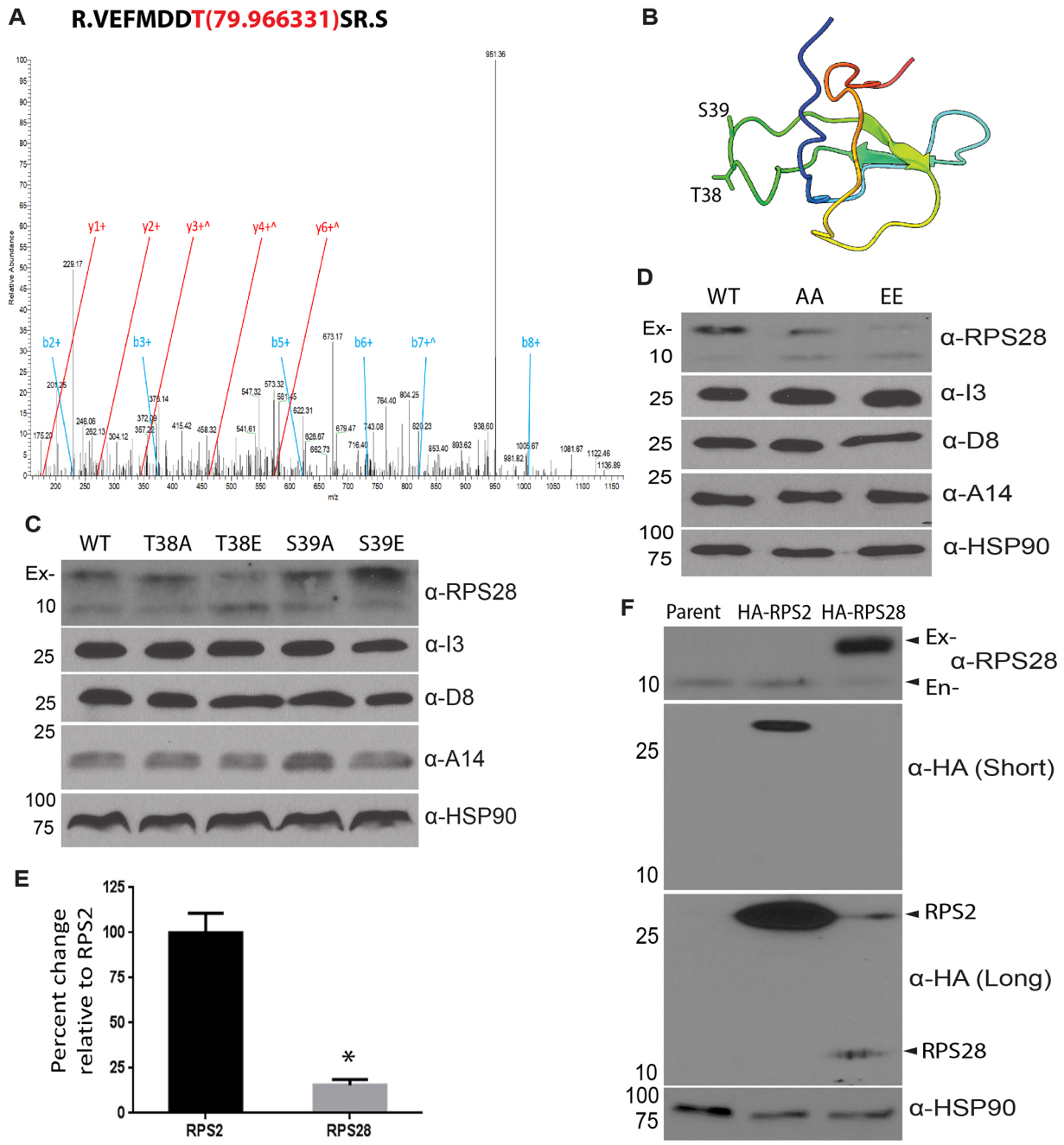

Fig. 5. RPS28 is expressed at low levels and its modification does not enhance infection in NHDFs. (A) MS/MS spectra of RPS28 peptides from GFP-TRAP ribosomes isolated from VacV-infected HAP1 cells. The peptide amino acid sequence, phosphorylated residue, b-series ions (blue), y-series ions (red), charge state (+), and ions that support phosphorylation (^) are all indicated. (B) Structural model of RPS28 with labeled amino acid residues identified as being phosphorylated during VacV infection. (C) Western blot analysis of NHDFs expressing HA–RPS28, or site-specific alanine (T38A; S39A) or glutamic acid (T38E; S39E) substitution mutants of HA–RPS28 infected with VacV (MOI=0.003) for 72 h. (D) Western blot analysis of NHDFs expressing HA-RPS28, or double alanine (AA) or glutamic acid (EE) substitution mutants of HA–RPS28 infected with VacV (MOI=0.003) for 72 h. (E) To estimate the relative abundance of RPS2 and RPS28 peptides identified by mass spectroscopy, spectra counts were used as a semi-quantitative measurement and the percentage difference between the total spectra count of identified RPS2 peptides compared to the total spectra count of RPS28 peptides was determined and displayed as the mean±s.e.m. percentage difference relative to the total spectra count of RPS2 (n=5). *P<0.05; NS, not statistically significant (unpaired Student's t-test). (F) Western blot analysis of NHDFs expressing HA–RPS2 or HA–RPS28 protein. Short and long exposures are shown to illustrate the relative difference in HA–RPS2 versus HA–RPS28 expression.

not exhibit a detectable mobility shift in samples infected with VacV when resolved by SDS-PAGE (Fig. 2A), preventing us from using this approach to map the modified site using alanine substitution mutants. As such, we expressed WT HA–RPS28 or single site mutants T38A or T38E, and S39A or S39E in NHDFs and tested their effects on VacV replication in spreading assays, as described for RPS2 lines above. WB analysis showed that alanine or glutamic acid substitutions at either site had no detectable impact on viral protein accumulation (Fig. 5C). To rule out the possibility that both sites were being modified, but not detected as simultaneous modifications in our mass spectrometry analysis, we repeated these spreading assays in pools of NHDFs expressing

Journal of Cell Science (2021) 134, jcs246603. doi:10.1242/jcs.246603

WT HA–RPS28 or double mutants, T38A/S39A or T38E/S39E. Again, WB analysis failed to detect any notable impact on viral protein accumulation in cells expressing either mutant (Fig. 5D).

While this data suggest that phosphorylation of RPS28 may be incidental and not functionally important for infection, several observations suggested that RPS28 may be expressed at sub-stoichiometric levels that further limit its potential to regulate infection or our ability to detect more nuanced roles in infection. Unlike other RPSs, endogenous RPS28 was extremely difficult to detect by WB analysis (Fig. 5C,D). In addition, our mass spectrometry analyses only detected RPS28 peptides at ∼15% of the level of those for other RPSs, such as RPS2 (Fig. 5E). These are obviously indirect observations that could simply reflect differences in the quality of the RPS28 antibody compared with those raised against other RPSs that we have used to date, and differences in peptide cleavage in our mass spectrometry analyses. However, HA–RPS28 was also expressed at very low levels; despite using the same viral vector, the same N-terminal tag location and the same anti-HA antibody to probe for expression of exogenous forms of RPS2 or RPS28 in NHDF pools, signal from HA–RPS28 was extremely weak compared with that for HA–RPS2 (Fig. 5F). Yet when these lines were probed with anti-RPS28 antibody, the exogenous HA–RPS28 protein was seen to be expressed at higher levels than the endogenous form (Fig. 5F). Cumulatively, these data suggest that RPS28 is expressed at low levels compared with other RPs, and the ability to overexpress this protein further supported the idea that it may be present at sub-stoichiometric levels on the ribosome, which allows overexpression of exogenous forms. Despite this, the relatively low levels of either endogenous or exogenous RPS28 compared with other RPs, such as RPS2, likely limits the impact of poxvirus-induced modifications to RPS28 on virus spread.

DISCUSSION

Our findings reveal the broader extent to which poxviruses actively manipulate ribosomes to facilitate their replication and add to our growing understanding of ribosome diversification.

Notably, RPS2 is located at the mRNA entry channel of the ribosome, while RPS28 is located at the mRNA exit channel on the opposing side to RACK1 (Fig. 6A,B). This suggests that both areas of the mRNA channel are directly targeted by poxviruses to control translation. Moreover, similar to RACK1 (Jha et al., 2017), the modifications to RPS2 and RPS28 occur in unstructured loop domains rather than structured strands or helices (Fig. 6C,D). While these unstructured regions are often considered as passive linkers between more structured domains in RPs that mediate protein–protein interactions, the effects of phosphorylation of either RACK1 (Jha et al., 2017) or RPS2, shown here, highlight the functional importance of these less-structured domains in regulating ribosome activity. Our recent structure modeling and biochemical testing suggests that negative charge in the RACK1 loop likely alters electrostatics at the exit channel, potentially remodeling this region to better accommodate translation of viral mRNAs that harbor unusual 5′ poly(A) leaders (Jha et al., 2017; Rollins et al., 2019). Our findings that phosphorylation events in the RPS2 unstructured domain enhances virus spread and translation of mRNAs with 5′ poly(A) leaders suggests that RPS2 functions analogously to RACK1, but at the mRNA entry channel. Our preliminary clash modeling found no evidence of predicted changes in electrostatics in the context of RPS2 phosphorylation. However, there are limitations to modeling unstructured regions, while it is also possible that phosphorylation of RPS2 functions in a distinct manner to control processes at the mRNA entry channel. While this remains to be tested, our data clearly show that poxviruses induce functionally important PTMs around the mRNA entry and exit channels to enhance their replication. Although modifications to

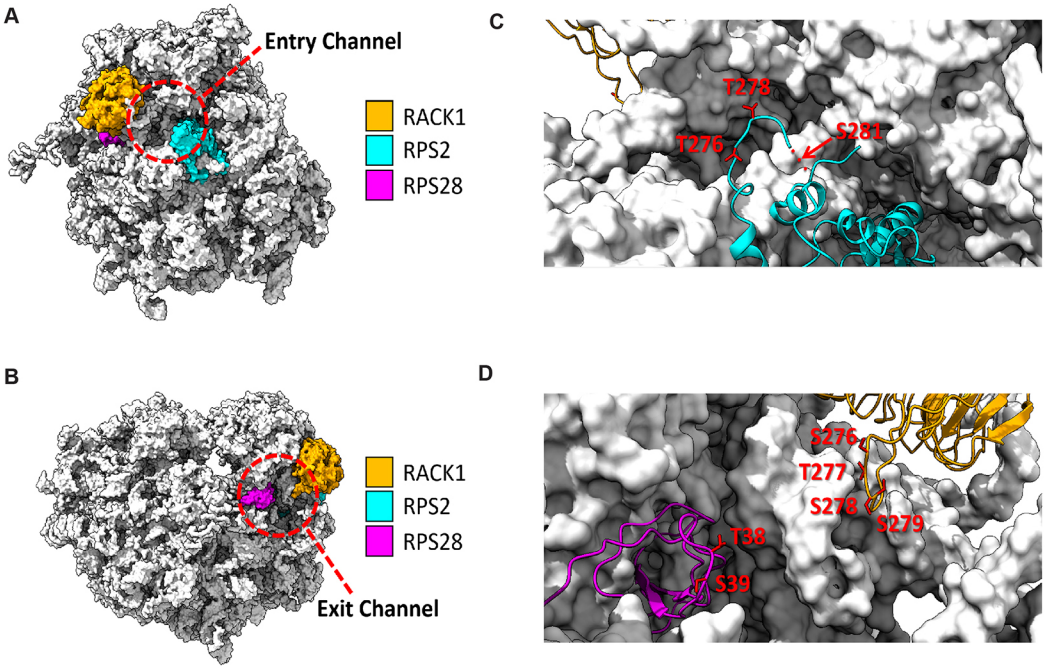

Fig. 6. Poxvirus-modified RPs are positioned at the mRNA entry and exit channels of the ribosome. (A) Structural model of the 80S ribosome facing toward the mRNA entry channel with RACK1 (orange), RPS2 (cyan), and RPS28 (magenta) highlighted. (B) Rotated structural model from A, showing the mRNA exit channel. (C) Higher magnification view of the entry channel showing the location of RPS2 residues that are phosphorylated during VacV infection. (D) Higher magnification view of the exit channel showing the location of RPS28 and RACK1 residues that are phosphorylated during VacV infection. Modified sites in RPS2, RPS28 and RACK1 shown in C and D lie within unstructured loops.

RPs could potentially alter ribosome biogenesis, cells infected with VacV wherein multiple RPs are modified simultaneously exhibit no gross changes in polysome profiles that would suggest defects in ribosome assembly (Dai et al., 2017 and our unpublished observations). RPs have been reported to have extra-ribosomal functions, although this may be limited to specific transformed cell types commonly used in research studies. Indeed, as discussed earlier, we and others do not detect appreciable levels of many RPs outside of ribosome fractions in the cell types used in these studies, and we detect no significant changes in overall translation in cells expressing phosphomimetics of RPS2, here, or of RACK1 previously (Jha et al., 2017; Rollins et al., 2019). Instead, our data suggests that the RP modifications detected in VacV-infected cells thus far serve to enhance the production of viral proteins by operating on the ribosome. Regardless of alternatives as to their most likely function on the ribosome, our findings clearly show that phosphorylation of proteins such as RPS2 plays an important role in increasing production of proteins encoded by mRNAs with poly(A) leaders and maximizing VacV replication. Finally, while the individual contribution of RPS2 phosphorylation is relatively small, most likely the combined effects of modifying multiple other RPs, such as RACK1 (Jha et al., 2017; Rollins et al., 2019), along with phosphorylation of eIFs (Walsh et al., 2008), cumulatively acts to more broadly regulate and maximize viral mRNA translation in infected cells.

In the case of RPS28, the modified loop region is juxtaposed with the modified loop of RACK1 (Fig. 6D). However, our data suggests that the modifications to RPS28 have little impact on viral protein production. Indeed, mass spectrometry studies have uncovered many PTMs to RPs, but many of these have yet to be shown to exert functional effects (Genuth and Barna, 2018). Our findings and the proximity of the RPS28 loop to that of RACK1 raises the possibility that modifications to RPS28 are inconsequential, and may in fact occur as 'collateral damage' while the viral kinase attempts to phosphorylate its nearby functional target, RACK1. However, we also find that RPS28 is expressed at very low levels, suggesting that it may be present only on a small fraction of ribosomes and therefore may function in a more nuanced fashion that is beyond our current detection limits. It is also possible that other cell types express higher levels of RPS28, where its modification might exert a greater functional impact on infection.

While these latter ideas remain to be tested, our findings reveal new modes of ribosome customization by poxviruses through phosphorylation of a loop domain in RPS2, and hint at potential sub-stoichiometric expression of RPS28 that may have as-yet-undetermined significance to translational control by contributing to intracellular heterogeneity in ribosome subunit composition (Shi et al., 2017; Genuth and Barna, 2018). This highlights the potential for studies of poxviruses to reveal new insights into how ribosomes can functionally diversify.

MATERIALS AND METHODS

Cell lines

HAP1 cells were purchased from Horizon, USA (C859) and grown in Iscove's modified Dulbecco's medium (IMDM; SH3022801) plus 5% Fetal bovine serum (FBS) and penicillin-streptomycin and maintained at 37°C in 5% CO_2. Certified primary normal human dermal fibroblasts (NHDFs) isolated from human male neonatal foreskin were purchased from Lonza (CC-2509) and grown in Dulbecco's Modified Eagle's Medium (DMEM; Fisher Scientific; MT15013CV) supplemented with 5% FBS, 2 mM L-Glutamine, and penicillin-streptomycin and maintained at 37°C in 5% CO_2. 293T, BSC40 and Vero cells were obtained from Dr I. Mohr, NYU School of Medicine and grown in DMEM supplemented with 5% FBS, 2 mM L-Glutamine, and penicillin-streptomycin and maintained at 37°C in 5% CO_2. Cells were verified mycoplasma free by Hoechst staining.

Viruses

The Western Reserve strain of Vaccinia virus (VacV) was grown and titered on BSC40 cells, as described previously (Walsh et al., 2008). Herpes simplex 1 virus (HSV-1) was grown and titrated on Vero cells as described previously (Walsh and Mohr, 2004). Vesicular stomatitis virus (VSV) was grown and titrated on Vero cells as previously described (Herdy et al., 2012). Temperature-sensitive (Ts) mutants and a corresponding wild-type (WT) strain of VacV were grown and titered on BSC40 cells at 32°C for use in infection assays, as described previously (Jha et al., 2017; Boyle and Traktman, 2004; Punjabi and Traktman, 2005; Rempel and Traktman, 1992; Wiebe and Traktman, 2007).

Plasmids, cloning, and mutagenesis

The N-terminally HA-tagged expression plasmid pCMV3-HA-RPS2 (SinoBiological; HG16154-NY) was used as a template to create lentiviral vectors and RPS2 mutants. PCR was first used to insert BamHI and EcoRI restriction sites within the major cloning site (MCS) of pCMV3 flanking the HA-RPS2 coding sequence (CDS) on the 5′ and 3′ regions respectively, using the primers: forward, 5′-GAGCGACGGATCCTAATACGACTCA-CTATAGG-3′ and reverse, 5′-CTGGCAACTAGAAGGCACAGGAATT-CAGCGTAC-3′.

pCMV3-HA-RPS2 was then digested with BamHI and EcoRI restriction enzymes and the HA-RPS2 CDS fragment was ligated into pQCXIP retroviral vector (Takara Bio USA; Retro-X™ Q Vector Set; Cat# 631516). To generate RPS2 mutants, gBlocks (Integrated DNA Technologies) were synthesized encoding a large C-terminal region of RPS2 harboring the following mutations: T276A, T278A, T278E, S281A, S281E, T278/S281A or T278/S281E (sequences provided in Table S1). Each gBlock was engineered with custom 5′ and 3′ regions outside of the NgoMVI and EcoRI restriction sites to allow amplification using PCR for subsequent sub-cloning using the primers: forward, 5′-CGAGTGTACGACTAAGTAGG-3′ and reverse, 5′-GGACTACACTCATGACATCG-3′.

The pQCXIP-HA-RPS2 vector contains two naturally occurring restriction sites: NgoMVI within the RPS2 CDS and EcoRI within the 3′ MCS, allowing for restriction-based replacement of this region in RPS2 with the mutant forms from amplified gBLOCKs. To do this, the gBlocks harboring the various mutations were digested with NgoMVI and EcoRI restriction enzymes and ligated directly into equivalently digested pQCXIP-HA-RPS2. To generate RPS28 mutants, an N-terminally HA-tagged form of RPS28 was synthesized entirely as a gBlock fragment as either a wild-type sequence or harboring the following mutations: T38A, T38E, S39A, S39E, T38/S39A, or T38/S39E and flanked with BamHI and EcoRI sites. The gBlock fragments were digested with BamHI and EcoRI and ligated into pQCXIP. Sequence fidelity of all cloning intermediates and final constructs was confirmed by in-house sequencing. gBLOCK Sequences are provided in Table S1.

Generation of stable cell lines

HAP1 RACK1-knockout cells and RACK1–eGFP expression vectors were generated as previously described (Jha et al., 2017). HAP1 RACK1-knockout cells expressing RACK1–eGFP were generated as follows: RACK1–eGFP cDNA was cloned into pLVX-IRES-Hygromycin plasmid (Takara Bio USA; cat. #632182) and lentivirus was generated by co-transfecting 293T cells with pLVX-Hygromycin RACK1-eGFP expression plasmid together with p8.91 (gag-pol; Dr Mojgan Naghavi, Department of Microbiology-Immunology, Northwestern University, USA) and p-VSV-G (envelope; Dr Mojgan Naghavi) plasmids. Lentiviral supernatants were then filtered through a 0.45 µm sterile syringe filter and HAP1 RACK1-knockout cells were transduced with lentivrus. Cells were selected with 100 µg/ml hygromycin and confirmed for expression by western blotting.

Retroviral vectors described above were used to generate NHDFs stably expressing RPS2 or RPS28. To make viral vectors, Lipofectamine 3000 (Thermo Fisher Scientific; L3000001) was used to transfect pQCXIP plasmids that expressed wild-type or mutant HA–RPS2 or HA–RPS28 into Phoenix-AMPHO retroviral packaging cells (ATCC; CRL-3213) grown on

10 cm dishes. Supernatant was collected at 48 and 72 h post transfection, and filtered through 0.45 µm filter, aliquoted and stored at −80°C until use. Low passage NHDFs were grown to ∼70% confluency in 10 cm dishes with no antibiotics and transduced with 2 ml of retroviral supernatant supplemented with 10 µg/ml polybrene in 3 ml of a 1:1 mix of DMEM and optiMEM (Thermo Fisher Scientific; 51985091). Following a 5 h incubation, the medium was replaced with 10 ml of 1:1 DMEM and optiMEM, and grown for 72 h. The DMEM:optiMEM was then replaced with DMEM supplemented with 4 µg/ml of puromycin for selection. After selection, cells were maintained in DMEM supplemented with 1 µg/ml of puromycin, and puromycin was removed from medium prior to performing all experiments.

Isolation of RACK1 complexes and mass spectrometry

For mass spectrometry analysis, eGFP or RACK1–eGFP were isolated from soluble cell lysates as follows: 3×10 cm dishes were seeded with HAP1 cells stably expressing exogenous eGFP or RACK1–eGFP. Cells were either mock infected or infected with VacV at a MOI 5 for 20 h, HSV-1 at a MOI 5 for 20 h, or VSV at a MOI 5 for 6 h (VSV replicates faster than VacV or HSV-1, and reaches late stages of infection within 6 h). Cells were then washed twice with ice-cold PBS, completely aspirating off the PBS. Cells were then scraped into lysis/wash buffer [50 mM HEPES pH 7.4, 150 mM NaCl, 0.5 mM $MgCl_2$, 2 mM EDTA, 2 mM Na_3VO_4, 25 mM glycerophosphate, 1.5% NP-40 and mini EDTA-free protease inhibitor (Roche)]. For a 10 cm dish, cells were scraped into 1 ml of lysis/wash buffer and transferred to an Eppendorf tube. Tubes were rocked in a cold room for 30–40 min to lyse cells. Lysates were then centrifuged at 10,000 ***g*** for 10 min at 4°C. Input samples were taken, and the remainder of the clarified lysate was transferred (taking care to avoid the pellet) to Sepharose resin covalently conjugated to GFP-binding protein (GFP-Trap; ChromoTek; cat. #gta-100); prior to this, GFP-TRAP resin was prepared by washing twice in 500 µl of ice-cold lysis/wash buffer. Pre-equilibrated beads were pelleted at 2000 rpm for 1 min for each wash, and the remaining lysis/wash buffer was aspirated when ready to add the precleared cell lysate. The lysate was incubated with GFP-TRAP beads on a rocker at 4°C for 4 h. Samples were then centrifuged at 2000 rpm for 1 min at 4°C. A flow-through sample was collected before the remaining sample was aspirated and beads were then washed three times in 500 µl of lysis/wash buffer, incubating at 4°C with rocking for 5 min and then centrifuging at 2000 rpm for 1 min at 4°C to pellet beads during each wash. After removing the final wash, beads were boiled for 3 min in Laemmli buffer to elute the GFP-bound proteins. Protein was then precipitated using trichloroacetic acid (TCA) as previously described (Link and LaBaer, 2011), and analyzed by LC-MS/MS to detect potential phosphorylation events. No enrichment of phosphopeptides was performed. The precipitated protein pellets were solubilized in 50 µl of 8 M urea in 50 mm ammonium bicarbonate for 1 h followed by the addition of 50 µl of 0.2% ProteaseMAX (Promega; Cat# V207A) for 1 h. Protein extracts were reduced and alkylated with the addition of 1 µl of 500 mM TCEP for 1 h followed by 2 µl of 500 mM iodoacetamide for 20 min in the dark. The reaction was quenched with the addition of 5 µl of 500 mM TCEP, followed by the addition of 215 µl 50 mM ammonium bicarbonate, 2.5 µl 1% ProteaseMAX and 1.0 µg Trypsin Gold (Promega; Cat# V528A). Samples were digested overnight in at 37°C and the following morning the digest was quenched with formic acid and subjected to C18 purification using Pierce Spin Columns (Thermo Fisher Scientific, cat. #89879). The peptides were quantified using a microBCA protein assay kit (Thermo Fisher Scientific; cat. #23235) and three micrograms were auto loaded on to the Thermo Ultimate 3000 UPLC pump via Acclaim Pepmap 100, 75 µm by 2 cm, nanoViper trap column (Thermo Fisher Scientific; cat. #164535) coupled to RSLC 75 µm by 50 cm nanoViper analytical column (Thermo Fisher Scientific; cat. #164942). The mobile phase consists of buffer A (97.9% H_2O with 2% acetonitrile and 0.1% formic acid) and buffer B (99.9% acetonitrile with 0.1% formic acid). The peptides were eluted off the analytical with increasing concentration of buffer B over the course of 2.5 h. with the following profile: 2–8% over 6 min, ramp to 8–24% over 6–70 min, ramp to 24–36% over 70–90 min, ramp to 36–55% over 90–100 min, ramp to 55–95% over 100–120 min, back to 95–2% for 120–150 min. The eluted peptides were electrosprayed from the stainless-steel emitter tip on the Nanospray Flex Ion Source at a voltage of 2000 V into Orbitrap Fusion Tribrid mass spectrometer for analysis. The MS parameters include: ion transfer tube temperature to 300°C, Easy-IC internal mass calibration, and the default charge state was set to 2 and cycle time was set to 3 s. Detector type was set to Orbitrap, with 60,000 resolution, with wide quad isolation, mass range was set to normal, scan range was set to 300–1500 (m/z), max injection time was set to 50 ms, AGC target was set to 200,000, microscans was set to 1, S-lens RF level was set to 60, without source fragmentation, and datatype was set to positive and centroid. Monoisotopic precursor selection was set as on and included charge states equal to 2–6 (and reject unassigned). Dynamic exclusion enabled and set to 1 for 30 s and 45 s exclusion duration at 10 ppm for high and low. Precursor selection decision was set to most intense, top 20, isolation window was set to 1.6, and scan range was set to auto normal, first mass was set to 110, collision energy was set to 30%. For collision-induced dissociation (CID), we used the ion trap (IT) detector, IT resolution was set to 30K, IT scan rate was set to rapid, max injection time was set to 75 ms, AGC target was set to 10,000, and Q was set to 0.25; finally, we injected ions for all available parallelizable time. Spectrum raw files were extracted into MS1 and MS2 files using the in-house program RawConverter (http://fields.scripps.edu/downloads.php), and the tandem mass spectra were searched against UniProt human database (downloaded on 25 March 2014). The search parameters included all fully and half-tryptic peptide candidates that fell within the mass tolerance window with unlimited missed cleavages and 50 pmm precursor tolerance with fragment mass tolerance of 600 ppm. Carbamidomethylation (+57.02146 Da) of cysteine was considered as a static modification and a differential modification of 79.9663 on serine, threonine or tyrosine with maximum number of internal differential modifications of 2. Further DTASelect filtering included minimum number of peptides and tryptic peptides per protein set to 1 and precursor delta mass cut off as 10. The false discovery rate (FDR) threshold was set to 1% and peptide FDRs were determined by using the reverse protein sequences contained in the target/decoy database and those peptides with FDR>1% were excluded from the analysis. All samples were directly compared using their measurements of abundance generated by IDCompare.

Virus infections and virus spreading assays

Infections with different viruses were performed at the MOIs and for the time periods indicated above or in figure legends. To determine effects on VacV replication at a low MOI, pools of NHDFs expressing N-terminal HA-tagged forms of RPS2 or RPS28 were infected with VacV at MOI 0.003 for 72 h at 37°C prior to being harvested in lysis buffer. Plaque assays were performed by infecting NHDFs at MOI 0.003 for 72 h at 37°C. Cells and supernatant were then collected and subjected to three freeze-thaw cycles, and levels of infectious virus were determined by serial dilution and titration on permissive BSC40 cells. For infection with temperature-sensitive (Ts) mutants of VacV, NHDF cells were infected at a MOI 10 and incubated at either 32°C or 39.5°C for 20 h post infection. Cells were harvested in lysis buffer and analyzed by WB analysis as described below.

RNAi and metabolic labeling

Pre-designed siRNAs were acquired from Life Technologies (Thermo Fisher Scientific): control siRNAs (AM4635), siRNA against RPS2 (siRNA1 ID 12402; siRNA2 ID 12314) and siRNA against RPS28 (siRNA1 ID 284684; siRNA2 ID 284683). HAP1 cells were transfected with 150 pmol/ml of siRNAs using RNAiMax (Invitrogen) and at 72 h post transfection, and then cells were infected with VacV at 0.5 MOI for 20 h. To metabolically label nascent protein, for 30 min prior to cell lysis, cultures were incubated in methionine- and cysteine-free DMEM (17-204-CL; Corning) supplemented with 40 mM HEPES and 35 µCi [^{35}S]methionine and [^{35}S]cysteine (NEG072; Amersham), as described previously (Walsh and Mohr, 2006). Whole-cell lysates were resolved by SDS-PAGE and gels were then fixed in a solution of 10% acetic acid and 50% methanol. Gels were then dried and exposed to X-ray film.

Western blotting

For WB analysis, cells were lysed in Laemmli buffer (62.5 mM Tris-HCl at pH 6.8, 2% SDS, 10% glycerol and 0.7 M β-mercaptoethanol) and the lysate was boiled for 3 min. Lysates were resolved using 12.5% polyacrylamide

Tris-glycine SDS-PAGE gels and transferred to a nitrocellulose membrane (GE Healthcare Life Sciences) at 57 V for 60 min (Mini Trans-Blot system, Bio-Rad), washed in Tris-buffered saline (TBS) containing 0.1% Tween 20 (TBS-T) and blocked (5% non-fat milk in TBS-T) prior to incubating with primary antibodies diluted in 3% BSA TBS-T gently rocking overnight at 4°C (primary antibodies are listed below and were diluted at 1:1000). The membranes were washed with TBS-T followed by incubation with the appropriate horseradish peroxidase (HRP)-conjugated secondary antibody (GE Healthcare Life Sciences; cat. #NA931V and #NA934V) diluted 1:2000 in TBS-T containing 5% non-fat milk for 1 h at room temperature with gently agitation. Membranes were washed in TBS-T and incubated with Pierce ECL western blotting substrate (Thermo Fisher Scientific) before being exposed to X-ray film.

The following antibodies were used in WB analysis: mouse anti-I3 (Dr David Evans, Li Ka Shing Institute of Virology, University of Alberta, Canada), mouse anti-D8 (Dr Paula Traktman, Department of Biochemistry and Molecular Biology, Medical University of South Carolina, USA), mouse anti-A14 (Dr Yan Xiang, Department of Microbiology, Immunology and Molecular Genetics, University of Texas Health Sciences Center San Antonio, USA), rabbit anti-gB (Dr Richard Longnecker, Department of Microbiology-Immunology, Northwestern University, USA), mouse anti-ICP4 (Abcam; cat. #Ab6514), mouse anti-VsV-G (Abcam; cat. #Ab50549), rabbit anti-RAPTOR (Abcam; cat. #ab40768), rabbit anti-GFP (Cell Signaling Technology; cat. #2956), rabbit anti-RACK1 (Cell Signaling Technology; cat. #5432), mouse anti-HA (Cell Signaling Technology; cat. #23675), rabbit anti-HSP90 (Cell Signaling Technology; cat. #4877s), rabbit anti-RPS2 (Thermo Fisher Scientific; cat. #PA5-30160), and rabbit anti-RPS28 (Thermo Fisher Scientific; cat. #PA5-45721).

Luciferase assay

NHDFs were grown on 12-well plates and electroporated with 200 ng plasmid DNA encoding luciferase reporter harboring 5′ poly(A) leaders as previously described (Rollins et al., 2019). At 20 h post electroporation, cells were washed with PBS and lysed with 200 µl luciferase cell culture lysis reagent (Promega, Madison). The lysates were centrifuged at 10,000 ***g*** for 2 min to clarify. Next, 20 µl supernatant was added to 96-well plate and luciferase activity was measured using a Spectramax microplate reader.

Phosphatase treatment of lysates

2.5 µl of 10× NEB buffer 3.1 (B7203S) together with either 0 µl, 2.5 µl or 5 µl of Shrimp Alkaline Phosphatase (rSAP) (NEB M0371L) at a concentration of 1000 units/ml was added to 20 µl of Laemmli lysate. Sterile water was inversely added at 5 µl, 2.5 µl and 0 µl respectively to maintain the same volume across samples. Lysates were incubated for 60 min at room temperature, and then analyzed by WB analysis.

Quantification and statistical analysis

GraphPad Prism 6.01 software was used to graph quantifications. Results are displayed as mean±s.e.m. For comparisons between groups, a Student's *t*-test was performed to determine the statistical significance. A *P*-value of <0.05 indicates that a group is statistically significant. In the figures, an asterisk indicates the statistical significance while an 'NS' denotes the quantification was not statistically significant. The numbers (n) of experiments are indicated in the figure legends of each experiment. Relative densitometry of protein levels were determined using imageJ version 1.52p. All experiments are $n=3$ unless stated otherwise in the figure legends.

Acknowledgements

We thank Ian Mohr, Paula Traktman, David Evans, Yan Xiang and Richard Longnecker for providing reagents.

Competing interests

The authors declare no competing or financial interests.

Author contributions

Conceptualization: S.D., D.W.; Methodology: S.D., M.G.R., H.A., N.K.; Formal analysis: S.D., M.G.R., N.K., J.N.S., D.W.; Investigation: S.D., M.G.R., H.A.; Resources: S.D., M.G.R.; Data curation: S.D., M.G.R., H.A., N.K.; Writing - original draft: S.D.; Writing - review & editing: M.G.R., D.W.; Visualization: S.D., M.G.R.; Supervision: J.N.S., D.W.; Project administration: J.N.S., D.W.; Funding acquisition: D.W.

Funding

This work was supported by a grant from the National Institutes of Health (NIH) R01AI127456 to D.W. and F32AI140566 to S.D. Deposited in PMC for release after 12 months.

Supplementary information

Supplementary information available online at https://jcs.biologists.org/lookup/doi/10.1242/jcs.246603.supplemental

References

Banham, A. H., Leader, D. P. and Smith, G. L. (1993). Phosphorylation of ribosomal proteins by the vaccinia virus B1R protein kinase. *FEBS Lett.* **321**, 27-31. doi:10.1016/0014-5793(93)80614-Z

Boyle, K. A. and Traktman, P. (2004). Members of a novel family of mammalian protein kinases complement the DNA-negative phenotype of a vaccinia virus ts mutant defective in the B1 kinase. *J. Virol.* **78**, 1992-2005. doi:10.1128/JVI.78.4.1992-2005.2004

Buendia, B., Person-Fernandez, A., Beaud, G. and Madjar, J. (1987). Ribosomal protein phosphorylation in vivo and in vitro by vaccinia virus. *Eur. J. Biochem.* **162**, 95-103. doi:10.1111/j.1432-1033.1987.tb10547.x

Ceci, M., Gaviraghi, C., Gorrini, C., Sala, L. A., Offenhäuser, N., Marchisio, P. C. and Biffo, S. (2003). Release of eIF6 (p27BBP) from the 60S subunit allows 80S ribosome assembly. *Nature* **426**, 579-584. doi:10.1038/nature02160

Cherry, S., Doukas, T., Armknecht, S., Whelan, S., Wang, H., Sarnow, P. and Perrimon, N. (2005). Genome-wide RNAi screen reveals a specific sensitivity of IRES-containing RNA viruses to host translation inhibition. *Genes Dev.* **19**, 445-452. doi:10.1101/gad.1267905

Cox, E. A., Bennin, D., Doan, A. T., O'toole, T. and Huttenlocher, A. (2002). RACK1 regulates integrin-mediated adhesion, protrusion, and chemotactic cell migration via Its Src-binding Site. *Mol. Biol. Cell* **14**, 658-669. doi:10.1091/mbc.e02-03-0142

Coyle, S. M., Gilbert, W. V. and Doudna, J. A. (2009). Direct link between RACK1 function and localization at the ribosome in vivo. *Mol. Cell. Biol.* **29**, 1626-1634. doi:10.1128/MCB.01718-08

Dai, A., Cao, S., Dhungel, P., Luan, Y., Liu, Y., Xie, Z. and Yang, Z. (2017). Ribosome profiling reveals translational upregulation of cellular oxidative phosphorylation mRNAs during vaccinia virus-induced host shutoff. *J. Virol.* **91**, e01858-e01816. doi:10.1128/JVI.01858-16

de la Cruz, J., Karbstein, K. and Woolford, J. L.Jr. (2015). Functions of ribosomal proteins in assembly of eukaryotic ribosomes in vivo. *Annu. Rev. Biochem.* **84**, 93-129. doi:10.1146/annurev-biochem-060614-033917

Dhungel, P., Cao, S. and Yang, Z. (2017). The 5′-poly(A) leader of poxvirus mRNA confers a translational advantage that can be achieved in cells with impaired cap-dependent translation. *PLoS Pathog.* **13**, e1006602. doi:10.1371/journal.ppat.1006602

Digiuseppe, S., Rollins, M. G., Bartom, E. T. and Walsh, D. (2018). ZNF598 Plays distinct roles in interferon-stimulated gene expression and poxvirus protein synthesis. *Cell Reports* **23**, 1249-1258. doi:10.1016/j.celrep.2018.03.132

Ferretti, M. B. and Karbstein, K. (2019). Does functional specialization of ribosomes really exist? *RNA* **25**, 521-538. doi:10.1261/rna.069823.118

Ferretti, M. B., Ghalei, H., Ward, E. A., Potts, E. L. and Karbstein, K. (2017). Rps26 directs mRNA-specific translation by recognition of Kozak sequence elements. *Nat. Struct. Mol. Biol.* **24**, 700-707. doi:10.1038/nsmb.3442

Fuchs, G., Petrov, A. N., Marceau, C. D., Popov, L. M., Chen, J., O'leary, S. E., Wang, R., Carette, J. E., Sarnow, P. and Puglisi, J. D. (2015). Kinetic pathway of 40S ribosomal subunit recruitment to hepatitis C virus internal ribosome entry site. *Proc. Natl. Acad. Sci. USA* **112**, 319. doi:10.1073/pnas.1421328111

Gallo, S., Ricciardi, S., Manfrini, N., Pesce, E., Oliveto, S., Calamita, P., Mancino, M., Maffioli, E., Moro, M., Crosti, M. et al. (2018). RACK1 Specifically regulates translation through its binding to ribosomes. *Mol. Cell. Biol.* **38**, e00230-e00218. doi:10.1128/MCB.00230-18

Garzia, A., Jafarnejad, S. M., Meyer, C., Chapat, C., Gogakos, T., Morozov, P., Amiri, M., Shapiro, M., Molina, H., Tuschl, T. et al. (2017). The E3 ubiquitin ligase and RNA-binding protein ZNF598 orchestrates ribosome quality control of premature polyadenylated mRNAs. *Nat. Commun.* **8**, 16056. doi:10.1038/ncomms16056

Genuth, N. R. and Barna, M. (2018). The discovery of ribosome heterogeneity and its implications for gene regulation and organismal life. *Mol. Cell* **71**, 364-374. doi:10.1016/j.molcel.2018.07.018

Gerbasi, V. R., Weaver, C. M., Hill, S., Friedman, D. B. and Link, A. J. (2004). Yeast Asc1p and mammalian RACK1 are functionally orthologous core 40S ribosomal proteins that repress gene expression. *Mol. Cell. Biol.* **24**, 8276. doi:10.1128/MCB.24.18.8276-8287.2004

Ghulam, M. M., Catala, M. and Abou Elela, S. (2019). Differential expression of duplicated ribosomal protein genes modifies ribosome composition in response to stress. *Nucleic Acids Res.* **48**, 1954-1968. doi:10.1093/nar/gkz1183

Herdy, B., Jaramillo, M., Svitkin, Y. V., Rosenfeld, A. B., Kobayashi, M., Walsh, D., Alain, T., Sean, P., Robichaud, N., Topisirovic, I. et al. (2012). Translational control of the activation of transcription factor NF-κB and production of type I interferon by phosphorylation of the translation factor eIF4E. *Nat. Immunol.* **13**, 543-550. doi:10.1038/ni.2291

Hertz, M. I., Landry, D. M., Willis, A. E., Luo, G. and Thompson, S. R. (2013). Ribosomal protein S25 dependency reveals a common mechanism for diverse internal ribosome entry sites and ribosome shunting. *Mol. Cell. Biol.* **33**, 1016. doi:10.1128/MCB.00879-12

Hinnebusch, A. G. (2014). The scanning mechanism of eukaryotic translation initiation. *Annu. Rev. Biochem.* **83**, 779-812. doi:10.1146/annurev-biochem-060713-035802

Jha, S., Rollins, M. G., Fuchs, G., Procter, D. J., Hall, E. A., Cozzolino, K., Sarnow, P., Savas, J. N. and Walsh, D. (2017). Trans-kingdom mimicry underlies ribosome customization by a poxvirus kinase. *Nature* **546**, 651-655. doi:10.1038/nature22814

Johnson, A. G., Lapointe, C. P., Wang, J., Corsepius, N. C., Choi, J., Fuchs, G. and Puglisi, J. D. (2019). RACK1 on and off the ribosome. *RNA* **25**, 881-895. doi:10.1261/rna.071217.119

Juszkiewicz, S. and Hegde, R. S. (2017). Initiation of quality control during Poly(A) translation requires site-specific ribosome ubiquitination. *Mol. Cell* **65**, 743-750.e4. doi:10.1016/j.molcel.2016.11.039

Juszkiewicz, S., Chandrasekaran, V., Lin, Z., Kraatz, S., Ramakrishnan, V. and Hegde, R. S. (2018). ZNF598 is a quality control sensor of collided ribosomes. *Mol. Cell* **72**, 469-481.e7. doi:10.1016/j.molcel.2018.08.037

Kaerlein, M. and Horak, I. (1978). Identification and characterization of ribosomal proteins phosphorylated in vaccinia-virus-infected HeLa cells. *Eur. J. Biochem.* **90**, 463-469. doi:10.1111/j.1432-1033.1978.tb12625.x

Komili, S., Farny, N. G., Roth, F. P. and Silver, P. A. (2007). Functional specificity among ribosomal proteins regulates gene expression. *Cell* **131**, 557-571. doi:10.1016/j.cell.2007.08.037

Kondrashov, N., Pusic, A., Stumpf, C. R., Shimizu, K., Hsieh, A. C., Ishijima, J., Shiroishi, T. and Barna, M. (2011). Ribosome-mediated specificity in Hox mRNA translation and vertebrate tissue patterning. *Cell* **145**, 383-397. doi:10.1016/j.cell.2011.03.028

Lafontaine, E., Miller, C. M., Permaul, N., Martin, E. T. and Fuchs, G. (2020). Ribosomal protein RACK1 enhances translation of poliovirus and other viral IRESs. *Virology* **545**, 53-62. doi:10.1016/j.virol.2020.03.004

Landry, D. M., Hertz, M. I. and Thompson, S. R. (2009). RPS25 is essential for translation initiation by the Dicistroviridae and hepatitis C viral IRESs. *Genes Dev.* **23**, 2753-2764. doi:10.1101/gad.1832209

Link, A. J. and Labaer, J. (2011). Trichloroacetic acid (TCA) precipitation of proteins. *Cold Spring Harb. Protoc.* **2011**, 993-994. doi:10.1101/pdb.prot5651

Majzoub, K., Hafirassou, M. L., Meignin, C., Goto, A., Marzi, S., Fedorova, A., Verdier, Y., Vinh, J., Hoffmann, J. A., Martin, F. et al. (2014). RACK1 controls IRES-mediated translation of viruses. *Cell* **159**, 1086-1095. doi:10.1016/j.cell.2014.10.041

Meade, N., Digiuseppe, S. and Walsh, D. (2019). Translational control during poxvirus infection. *WIREs RNA* **10**, e1515. doi:10.1002/wrna.1515

Nishiyama, T., Yamamoto, H., Uchiumi, T. and Nakashima, N. (2007). Eukaryotic ribosomal protein RPS25 interacts with the conserved loop region in a dicistroviral intergenic internal ribosome entry site. *Nucleic Acids Res.* **35**, 1514-1521. doi:10.1093/nar/gkl1121

Punjabi, A. and Traktman, P. (2005). Cell biological and functional characterization of the vaccinia virus F10 kinase: implications for the mechanism of virion morphogenesis. *J. Virol.* **79**, 2171-2190. doi:10.1128/JVI.79.4.2171-2190.2005

Rempel, R. E. and Traktman, P. (1992). Vaccinia virus B1 kinase: phenotypic analysis of temperature-sensitive mutants and enzymatic characterization of recombinant proteins. *J. Virol.* **66**, 4413-4426. doi:10.1128/JVI.66.7.4413-4426.1992

Rollins, M. G., Jha, S., Bartom, E. T. and Walsh, D. (2019). RACK1 evolved species-specific multifunctionality in translational control through sequence plasticity within a loop domain. *J. Cell Sci.* **132**, jcs228908. doi:10.1242/jcs.228908

Romano, N., Veronese, M., Manfrini, N., Zolla, L. and Ceci, M. (2019). Ribosomal RACK1 promotes proliferation of neuroblastoma cells independently of global translation upregulation. *Cell. Signal.* **53**, 102-110. doi:10.1016/j.cellsig.2018.09.020

Sanz, E., Yang, L., Su, T., Morris, D. R., Mcknight, G. S. and Amieux, P. S. (2009). Cell-type-specific isolation of ribosome-associated mRNA from complex tissues. *Proc. Natl. Acad. Sci. USA* **106**, 13939-13944. doi:10.1073/pnas.0907143106

Schmitt, K., Smolinski, N., Neumann, P., Schmaul, S., Hofer-Pretz, V., Braus, G. H. and Valerius, O. (2017). Asc1p/RACK1 connects ribosomes to eukaryotic phosphosignaling. *Mol. Cell. Biol.* **37**. doi:10.1128/MCB.00279-16

Sengupta, J., Nilsson, J., Gursky, R., Spahn, C. M. T., Nissen, P. and Frank, J. (2004). Identification of the versatile scaffold protein RACK1 on the eukaryotic ribosome by cryo-EM. *Nat. Struct. Mol. Biol.* **11**, 957-962. doi:10.1038/nsmb822

Shi, Z. and Barna, M. (2015). Translating the genome in time and space: specialized ribosomes, RNA regulons, and RNA-binding proteins. *Annu. Rev. Cell Dev. Biol.* **31**, 31-54. doi:10.1146/annurev-cellbio-100814-125346

Shi, Z., Fujii, K., Kovary, K. M., Genuth, N. R., Rost, H. L., Teruel, M. N. and Barna, M. (2017). Heterogeneous ribosomes preferentially translate distinct subpools of mRNAs genome-wide. *Mol. Cell* **67**, 71-83.e7. doi:10.1016/j.molcel.2017.05.021

Simms, C. L., Yan, L. L. and Zaher, H. S. (2017). Ribosome collision is critical for quality control during No-Go decay. *Mol. Cell* **68**, 361-373.e5. doi:10.1016/j.molcel.2017.08.019

Simsek, D. and Barna, M. (2017). An emerging role for the ribosome as a nexus for post-translational modifications. *Curr. Opin. Cell Biol.* **45**, 92-101. doi:10.1016/j.ceb.2017.02.010

Simsek, D., Tiu, G. C., Flynn, R. A., Byeon, G. W., Leppek, K., Xu, A. F., Chang, H. Y. and Barna, M. (2017). the mammalian ribo-interactome reveals ribosome functional diversity and heterogeneity. *Cell* **169**, 1051-1065.e18. doi:10.1016/j.cell.2017.05.022

Sundaramoorthy, E., Leonard, M., Mak, R., Liao, J., Fulzele, A. and Bennett, E. J. (2017). ZNF598 and RACK1 regulate mammalian ribosome-associated quality control function by mediating regulatory 40S ribosomal ubiquitylation. *Mol. Cell* **65**, 751-760.e4. doi:10.1016/j.molcel.2016.12.026

Sung, M.-K., Reitsma, J. M., Sweredoski, M. J., Hess, S. and Deshaies, R. J. (2016). Ribosomal proteins produced in excess are degraded by the ubiquitin-proteasome system. *Mol. Biol. Cell* **27**, 2642-2652. doi:10.1091/mbc.e16-05-0290

van de Waterbeemd, M., Tamara, S., Fort, K. L., Damoc, E., Franc, V., Bieri, P., Itten, M., Makarov, A., Ban, N. and Heck, A. J. R. (2018). Dissecting ribosomal particles throughout the kingdoms of life using advanced hybrid mass spectrometry methods. *Nat. Commun.* **9**, 2493. doi:10.1038/s41467-018-04853-x

Walsh, D. and Mohr, I. (2004). Phosphorylation of eIF4E by Mnk-1 enhances HSV-1 translation and replication in quiescent cells. *Genes Dev.* **18**, 660-672. doi:10.1101/gad.1185304

Walsh, D. and Mohr, I. (2006). Assembly of an active translation initiation factor complex by a viral protein. *Genes Dev.* **20**, 461-472. doi:10.1101/gad.1375006

Walsh, D., Arias, C., Perez, C., Halladin, D., Escandon, M., Ueda, T., Watanabe-Fukunaga, R., Fukunaga, R. and Mohr, I. (2008). Eukaryotic translation initiation factor 4F architectural alterations accompany translation initiation factor redistribution in poxvirus-infected cells. *Mol. Cell. Biol.* **28**, 2648-2658. doi:10.1128/MCB.01631-07

Warner, J. R. and Mcintosh, K. B. (2009). How common are extraribosomal functions of ribosomal proteins? *Mol. Cell* **34**, 3-11. doi:10.1016/j.molcel.2009.03.006

Wiebe, M. S. and Traktman, P. (2007). Poxviral B1 kinase overcomes barrier to autointegration factor, a host defense against virus replication. *Cell Host Microbe* **1**, 187-197. doi:10.1016/j.chom.2007.03.007

Xu, A. and Barna, M. (2020). Cleaning up stalled ribosome-translocon complexes with ufmylation. *Cell Res.* **30**, 1-2. doi:10.1038/s41422-019-0249-1

Xu, G., Greene, G. H., Yoo, H., Liu, L., Marques, J., Motley, J. and Dong, X. (2017). Global translational reprogramming is a fundamental layer of immune regulation in plants. *Nature* **545**, 487-490. doi:10.1038/nature22371

Xue, S., Tian, S., Fujii, K., Kladwang, W., Das, R. and Barna, M. (2015). RNA regulons in Hox 5′ UTRs confer ribosome specificity to gene regulation. *Nature* **517**, 33-38. doi:10.1038/nature14010

Yamada, S. B., Gendron, T. F., Niccoli, T., Genuth, N. R., Grosely, R., Shi, Y., Glaria, I., Kramer, N. J., Nakayama, L., Fang, S. et al. (2019). RPS25 is required for efficient RAN translation of C9orf72 and other neurodegenerative disease-associated nucleotide repeats. *Nat. Neurosci.* **22**, 1383-1388. doi:10.1038/s41593-019-0455-7